# Fabrication of Anode Supported Thick Film Ceria Electrolytes for IT-SOFCs

**Abhishek Jaiswal and Eric D. Wachsman**
Department of Materials Science and Engineering, University of Florida, Gainesville, FL32611, USA

**Abstract.** Anode supported thick film ceria electrolyte unit cells were fabricated using a colloidal dip coating method for IT-SOFCs. Pre-sintering temperature of the anode substrate and the final sintering temperature were found to be the primary parameters determining the density of the film. With Ni-$Ce_{0.89}Gd_{0.11}O_{2-\delta}$ cermet anode, $La_{0.6}Sr_{0.4}Co_{0.2}Fe_{0.8}O_3$ cathode and 15 μm $Ce_{0.89}Gd_{0.11}O_{2-\delta}$ electrolyte, the cells were tested in a fuel cell configuration with air at the cathode and moist $H_2$ at the anode. At 650 °C, the cell indicated a maximum power density of ~0.27 W/cm$^2$ at a current density of 0.62 A/cm$^2$. Cell performance was compared with oxygen at the cathode and the cell indicated a maximum power density of ~0.50 W/cm$^2$ at 1.14 A/cm$^2$, 650 °C. Activation energy for the area specific resistance (ASR) of the cell suggests that with air at cathode, the cell performance was limited by gaseous diffusion at cathode and with oxygen at cathode, by oxygen ion transport across the electrolyte.

## 1. Introduction

Solid oxide fuel cells (SOFCs) are electrochemical devices that convert the chemical energy of a fuel into electrical energy in a clean, cheap and efficient way. State of the art SOFCs employ yttria stabilized zirconia (YSZ) as the electrolyte material operating at 700-1000 °C. High operation temperatures are required to overcome the resistive loss across the YSZ electrolyte. There is considerable driving force to reduce the operating temperatures of SOFCs to 500-700 °C. Advantages include use of cheap ferritic stainless steel as the interconnect material, lower operating cost and faster starting times for mobile applications [1-4].

Towards reducing the operating temperatures of SOFCs, two approaches have been actively pursued. The first approach is towards finding better electrolyte (with high ionic conductivity and high ionic transference number) and better electrode (with high catalytic activity and high mixed conductivity) materials. At the same temperature, doped ceria shows oxygen ion conductivity significantly higher than that of YSZ [5]. However, doped ceria is thermodynamically unstable in the anode atmosphere of the fuel cell due to reduction from $Ce^{4+}$ to $Ce^{3+}$ valence state. The polaronic charge transfer on the mixed-valent $Ce^{4+}/Ce^{3+}$ array results in electronic conduction inside the electrolyte, which under fuel cell conditions results in an internal short circuit and a lower available power than theoretical [6]. It has been shown that on lowering the operating temperatures this internal short circuit loss across doped ceria decreases due to a wider electrolytic domain, making doped ceria one of the most promising electrolyte materials for IT-SOFCs [4].

The second approach towards reducing the operating temperatures of SOFCs is by reducing the thickness of the electrolyte and attaining higher power densities at lower temperatures in cells with electrode supported electrolytes [7]. For processing of thick films on porous supports, the colloidal route has advantages over other film deposition techniques like vapor deposition (CVD/-EVD) and chemical routes (sol gel) in its simplicity, cost-effectiveness, flexibility (thickness ranging from 10-100 μm can be deposited) and upscalibility [8]. Also, exceptional performance has been reported for SOFCs fabricated from colloidal deposition technique by de Souza et al. and Kim et al. [9,10] using a 10 μm thick YSZ electrolyte.

Fabrication and initial performance results of an anode supported ceria electrolyte unit cell are reported in this communication. A colloidal dip coating method was used

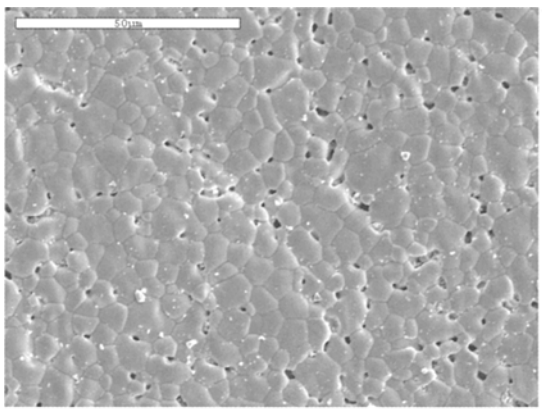

(a) 800 °C

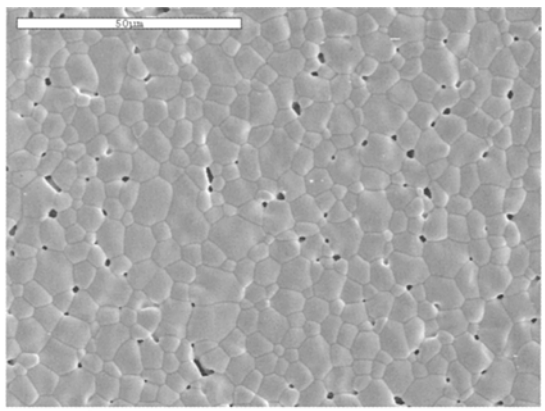

(b) 850 °C

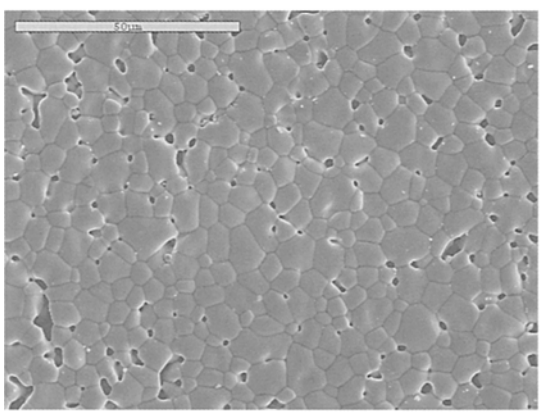

(c) 900 °C

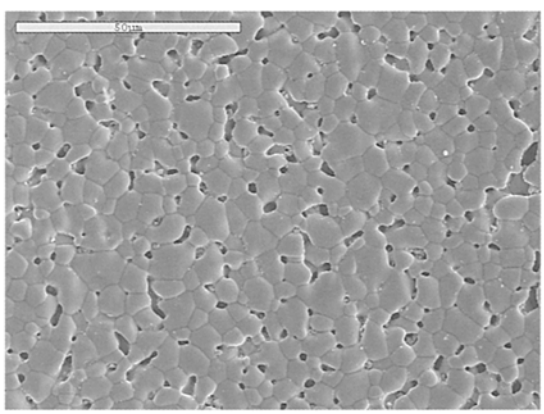

(d) 1000 °C

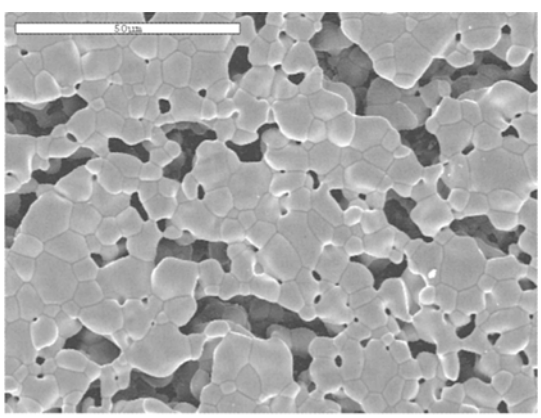

(e) 1100 °C

Fig. 1 (a)-(e). Representative microstructures of the GDC film under different pre-sintering conditions for a 1600 °C final sintering.

to fabricate the ceria films. Fabrication of dense thick films of ceria on porous anodes was achieved by varying the pre-sintering temperature of the anode substrate and final sintering temperature of the electrolyte coated substrate, which results in an optimum condition where the magnitude of shrinkage in the substrate is similar to that of the film.

Ni-doped ceria cermet and $La_{0.6}Sr_{0.4}Co_{0.2}Fe_{0.8}O_3$ was chosen as the anode material and the cathode material, respectively. Doped ceria is a mixed ionic electronic conductor under reducing conditions at the anode and hence, the reaction zone will not be restricted to the interface of the anode electrocatalyst and the electrolyte, leading to enhanced performance of the anode. Chemical

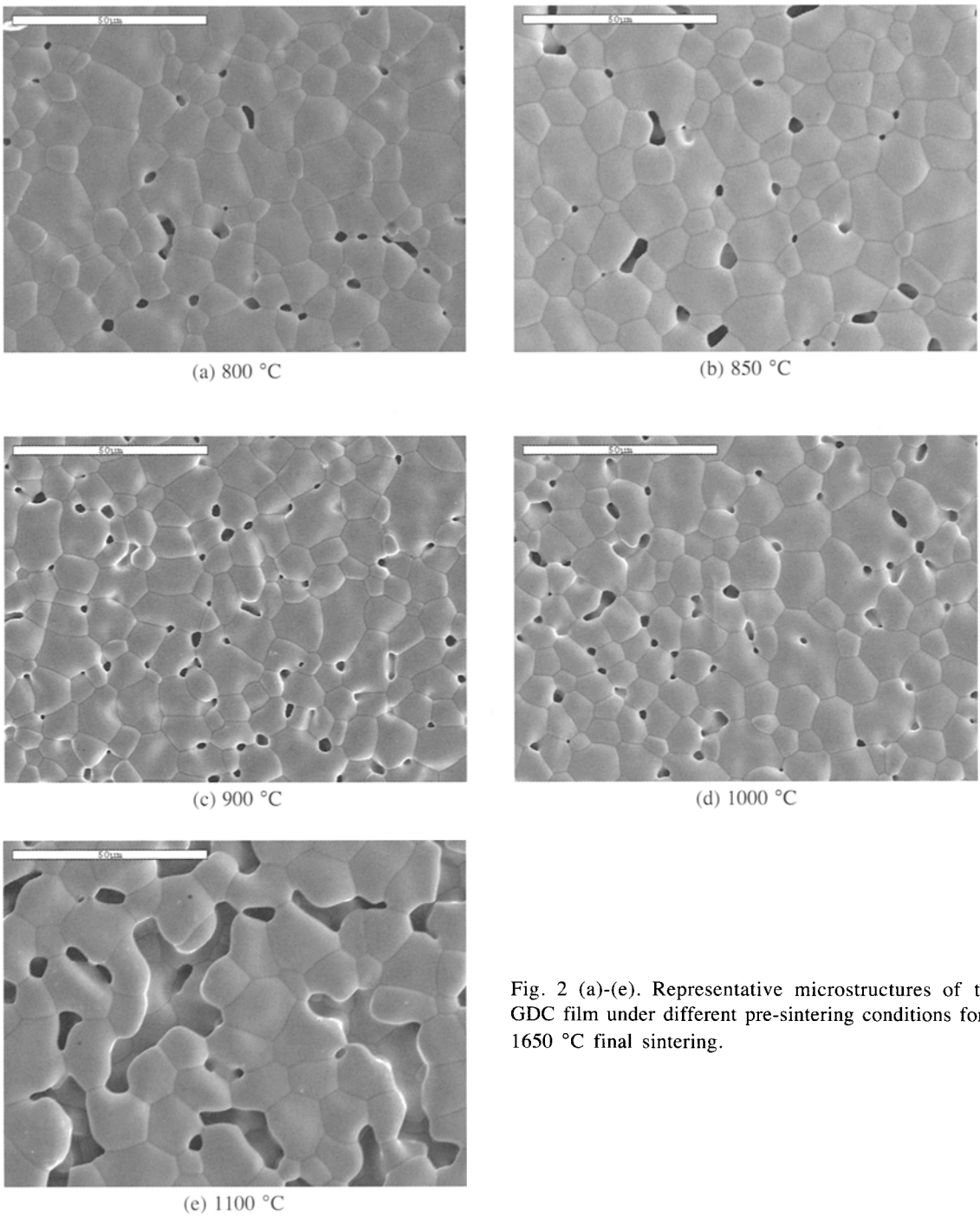


Fig. 2 (a)-(e). Representative microstructures of the GDC film under different pre-sintering conditions for a 1650 °C final sintering.

composition and microstructure plays an important role in the performance of the electrodes, as shown by Ohara et al. [11]. They studied the performance of Ni-samaria doped ceria cermet anodes as a function of Ni content and found that at 800 °C, a cermet with a Ni content of around 50 vol% showed the lowest anodic polarization (~30 mV at 300 mA/cm$^2$). Thus, in this work a NiO-gadolinium doped ceria (GDC) anode was fabricated with Ni content of 50 vol.%. Reduction of NiO to Ni was accomplished insitu in the cell, which would generate ~26 % porosity in the structure. La(Sr)Co(Fe)$O_{3-\delta}$ (LSCF) has been extensively studied as a candidate cathode material for SOFCs [12,13]. LSCF is a good electronic conductor and also shows fast oxygen surface exchange with high

oxygen ion conductivity [14]. They appear to be chemically stable with ceria electrolytes as the pyrochlore compound $La_2Ce_2O_7$ does not exist [15]. Among the family, the Fe rich compositions are more attractive than Co rich compositions as they have lower thermal expansion coefficient and hence, better matched with ceria electrolytes [16].

## 2. Experimental Procedure

11 mol% gadolinium doped ceria powder (GDC $d_{50}$ = 0.64 μm, SA = 24 $m^2$/gm) from Rhodia and NiO (–325 #) powder from Alfa-Aeaser were mixed and ball milled for 24 hours with zirconia ball media in ethanol. The mixed NiO-GDC powder was dried, sieved with 140 # stainless steel mesh and pressed uniaxially at pressures of 39.3 MPa to form discs of 1.25 inches diameter. The green bodies were then pre-sintered at temperatures between 800 °C and 1100 °C. For the colloidal suspensions, GDC powder was suspended in iso-proponal with poly-vinyl butyral (PVB) as binder, equal to 5-7 wt.% of the powder. The suspension was sonicated in an ultrasonic bath to disperse the GDC powder. The GDC electrolyte layer was deposited on the pre-sintered NiO-GDC discs by dip-coating and finally sintered at temperatures between 1400 °C and 1650 °C. Multiple coatings of the sol was done to get thicker films. Some anode substrates were reduced in $H_2$ atmosphere at 800 °C for 5 hours to measure the anode density after reduction, using the Archimede's principle.

$La_{0.6}Sr_{0.4}Co_{0.2}Fe_{0.8}O_3$ (LSCF $d_{50}$ = 0.7 μm, SA = 6 $m^2$/gm) from Praxiar Speciality Chemicals was mixed with α-terpinol, di-butyl pthalate, PVB and ethanol to from the cathode paste. The paste was screen printed on the sintered GDC electrolyte film. The cathode layer was dried at 100 °C and finally sintered at temperatures between 750 °C and 1100 °C. Finally, Pt mesh with gold wires spot welded was attached to the anode with Pt paste and to the cathode with the cathode paste, which were then sintered to act as current collectors. The active cathode and anode areas were approximately 1.6 $cm^2$ and 4.5 $cm^2$, respectively.

The samples were characterized using XRD (APD-3720) and SEM (JEOL-6400) in surface and cross-sectional view. The percentage porosity in the GDC films was estimated by stereological point counting method using a 25 point grid.

Unit cells were sealed on an alumina tube with Aremco cement (516 & 571), as described by de Souza et al. [9] and gold lead wires were attached to the cell. The cells were tested with air or oxygen at the cathode side and $H_2$/3%$H_2O$ at the anode side at flow rates of 10-30 sccm between 500 °C and 700 °C. The flow rate at the anode and cathode was kept equal. I-V characteristics of the cells were measured using an electrochemical interface (Solartron 1287). For the I-V characteristics each data point was collected after 10 minutes to attain a stable value. To measure the oxygen ion conductivity of the GDC electrolyte in air, impedance spectroscopy using Solartron 1260 was done on symmetrical cells consisting of GDC electrolyte and Pt electrodes.

## 3. Results and Discussion

For SOFC applications, the electrode needs to be sufficiently porous to allow for gaseous diffusion and the electrolyte needs to be highly dense to act as a barrier for the fuel gases and oxidant on the two electrodes. Surface microstructures of the sintered ceria film under different pre-sintering conditions (800-1100 °C for 4 hours) and different final sintering conditions (1600 °C for 6 hours and 1650 °C for 10 hours) are shown in Fig. 1(a)-(e) and Fig. 2(a)-(e). Figure 3 shows the percentage porosity of the GDC film under these sintering profiles. For each condition, the volume fraction of the porosity was estimated by the mean fraction of the points which lie on the pores. The error bars correspond to the standard deviation of the mean. Varying the pre-sintering temperature leads to minima in porosity in the GDC film at 850 °C for both the final sintering temperatures of 1600 °C and 1650 °C, with mean values of 1.97 % and

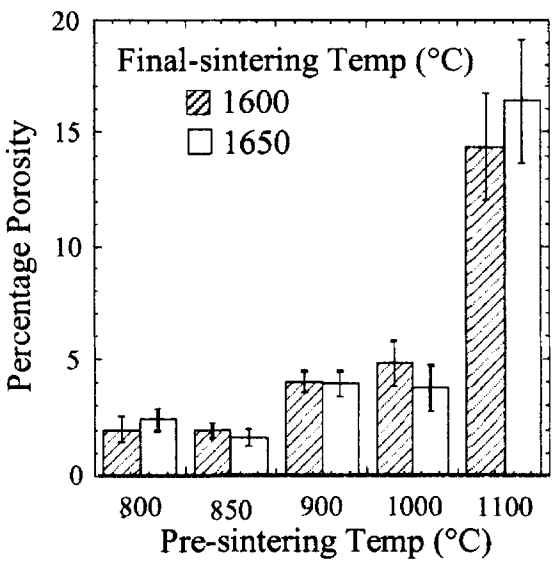


Fig. 3. Porosity in the GDC film as a function of the pre-sintering and final sintering temperature.

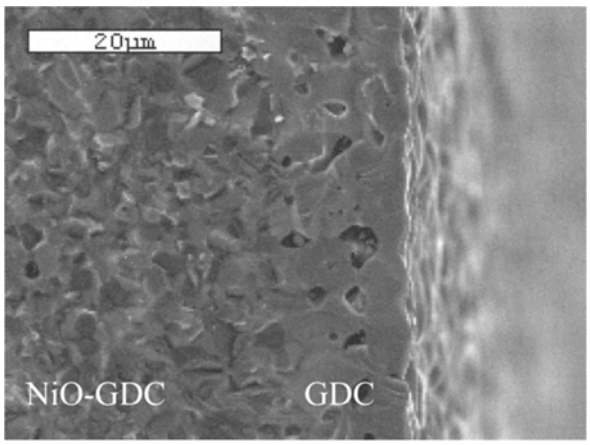


900 °C

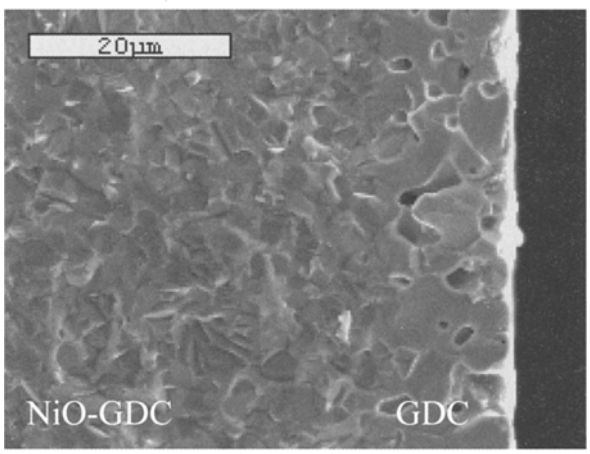


1000 °C

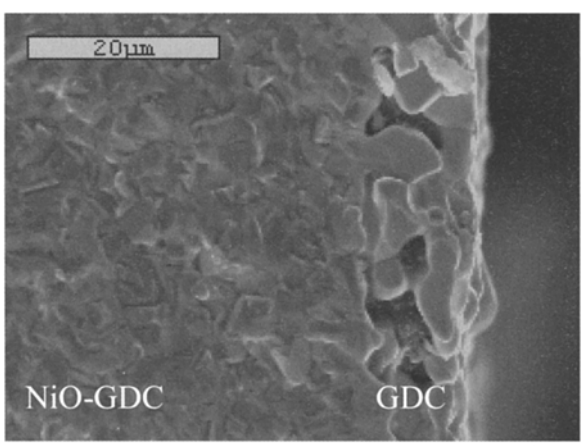


1100 °C

Fig. 4 (a)-(c). Cross-sectional microstructures of the GDC film under different pre-sintering conditions for a 1600 °C final sintering.

1.67 %, respectively. At higher pre-sintering temperature, the non-shrinking nature of the anode substrate leads to constrained sintering of the film and to a highly porous microstructure. At ~850 °C, the shrinkage in the substrate is similar to that of the film resulting in a comparatively denser film. Final sintering at 1650 °C leads to coarsening of the microstructure as shown in Fig. 2. Both the grain and pore size increase and become almost twice the size to that sintered at 1600 °C. Bigger pore size in the thin film electrolyte microstructure will have greater chances of failure in partitioning the fuel and air atmospheres. Also, thermodynamic studies on film stability have shown that, the film thickness should be larger than the grain size of the film for the film to be stable [17]. Otherwise, the film would lower its energy by breaking into isolated islands and exposing the substrate. The sampling done to measure the porosity in the film may not be ideal as the surface porosity of the film might be different from that of the bulk. However, it was assumed that the trends in the surface density of the film will be similar to that of the bulk density. Cross-sectional micrographs of the films seem to support the argument, as can be seen in Fig. 4. Efforts to reduce the final sintering temperature to avoid the co-sintering of the anode resulted in a highly porous film as show in Fig. 5 for the film pre-sintered at 850 °C and finally sintered at 1400 °C. Hence, it was decided to work with films pre-sintered at 850 °C and finally sintered at 1600 °C for I-V measurements in a fuel cell configuration.

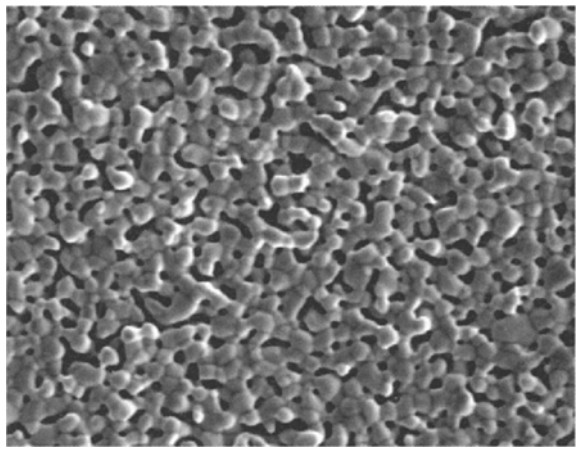

Fig. 5. Surface microstructure of the GDC film after 850 °C pre-sintering and 1400 °C final sintering.

The density of the anode substrate after sintering at 1600 °C was measured to be 6.72 gm/cc (~97 % of the theoretical density). On exposure to $H_2$ atmosphere at 800 °C, NiO in the anode reduced to Ni leading to an open porosity of ~20 % and a total porosity of ~29 % in the structure. Figures 6 (a) and (b) show the surface and the cross-sectional micrographs of the anode after reduction in back scattered electron mode, respectively. Sintering at

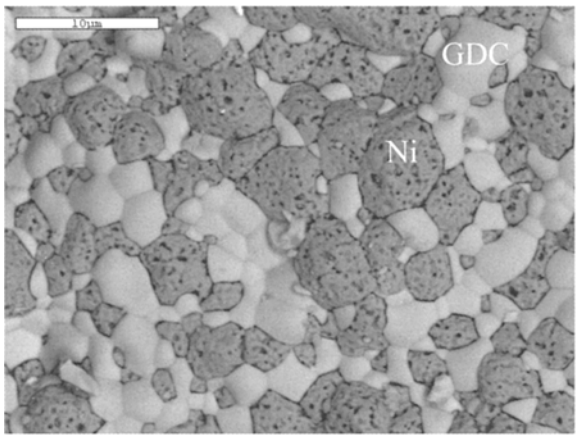


(a)

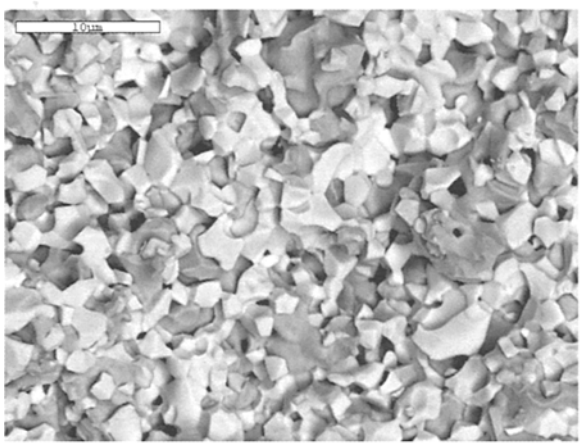

(b)

Fig. 6. Surface (a) and cross-sectional (b) microstructure of reduced Ni-GDC anode.

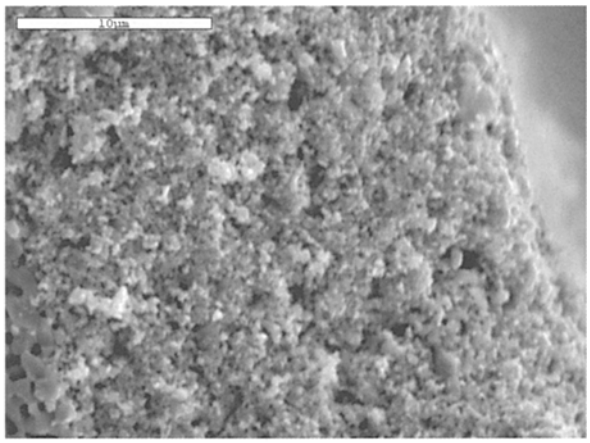

(a)

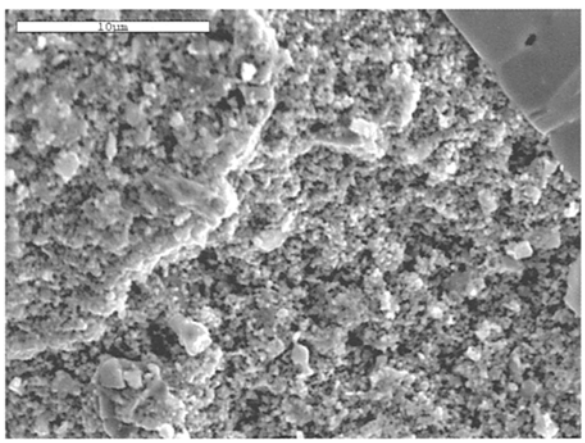

(b)

Fig. 7. Cross-sectional microstructure of LSCF cathode sintered at (a) 750 °C & (b) 900 °C.

1600 °C has lead to a coarsened microstructure with low concentration of triple phase boundaries (TPBs) and low porosity in the anode structure. The porosity at the surface is enclosed within Ni grains, while in the cross-section it appears to be more uniformly distributed. Also, coarse NiO grains might result in the incomplete reduction to Ni [18]. The reduced anode however, was conductive at room temperature and the XRD patterns did not show any peaks for NiO within the detection limits of the instrument. Further, improvement may be possible by reducing the final sintering temperature of the ceria films to avoid the sintering of the anode and by addition of pore-formers in the anode composition to improve porosity in the structure.

The high surface area LSCF powder had high sinterability and densified very easily at moderate temperature. Similar results were observed by Murray et al. [14]. Figures 7 (a), (b) show cross-sectional microstructures of the LSCF cathode sintered at 750 °C and 900 °C for 1 hour. The cathodes have insufficient porosity and for the I-V measurements a cathode sintered

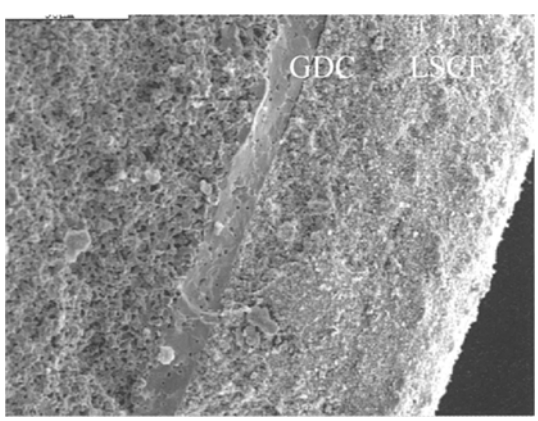


Fig. 8. Cross-sectional microstructure of tested unit cell - Ni-GDC anode (~1 mm) / GDC electrolyte (~15 μm) / LSCF cathode (~85 μm).

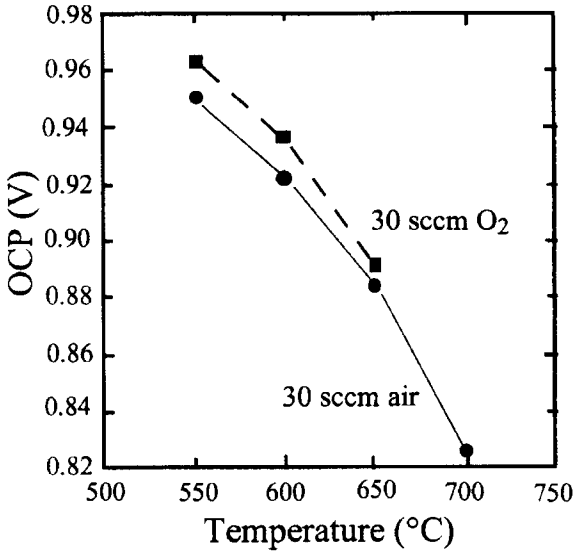


Fig. 9. Open circuit potential (OCP) of the cell as function of temperature.

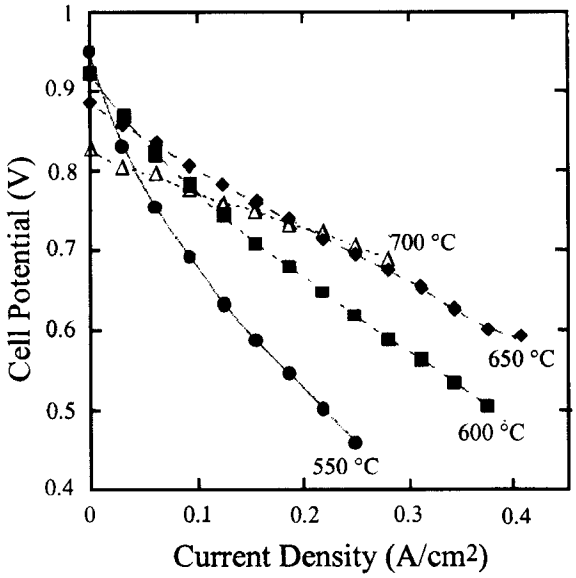


Fig. 11. I-V characteristics of the cell with air at the cathode.

at 750 °C was used. Figure 8 shows the fractured cross-section of a tested unit cell with the reduced Ni-GDC anode (~1 mm), GDC electrolyte (~15 μm) and LSCF cathode (~85 μm).

The open circuit potential (OCP) and power density of the cell were measured as a function of temperature, the cathode gas atmosphere and flow rate. Figures 9 and 10 are plots of OCP and average oxygen ion transference number vs. temperature of the cell, respectively. The electrolytic domain of ceria reduces and its ionic transference number decreases with increasing temperatures resulting in a lower OCP. With oxygen at the cathode, the cell showed higher OCP in comparison with air as expected. However, the theoretical OCP increased even more and the average transference number of the cell with oxygen was slightly lower than that of air. This indicates that electrode polarization effects are present even under the open circuit conditions due to the electronic leakage in ceria electrolytes.

Figure 11 shows the I-V characteristics of the cell with air at the cathode. In the open circuit conditions, the cell potential decreased on increasing the temperature as shown in Fig. 9. On drawing current, the cell potential decreased because of the various polarization losses across the cell. At 550 °C, the curvature in the plot at low current densities suggests that there is some activation

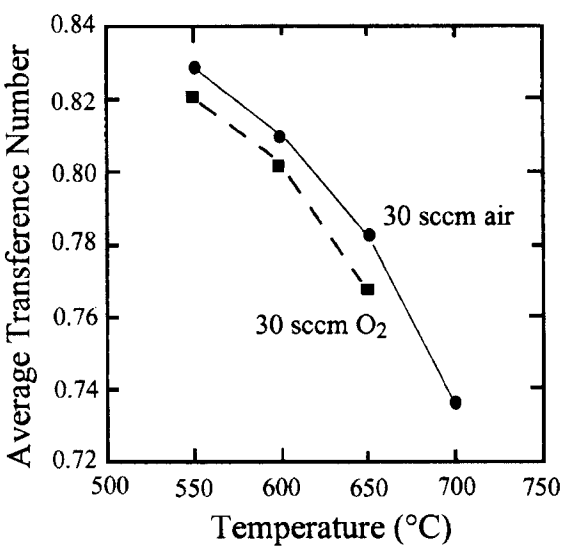


Fig. 10. Average oxygen ion transference number of GDC electrolyte as function of temperature.

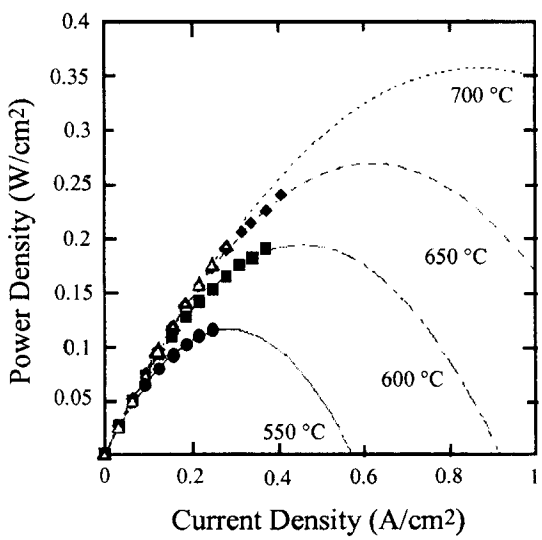


Fig. 12. Power Density of the cell with air at the cathode.

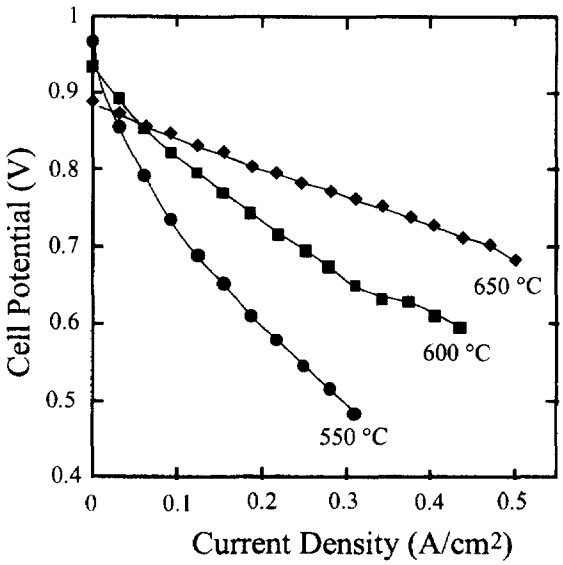


Fig. 13. I-V characteristics of the cell with oxygen at the cathode.

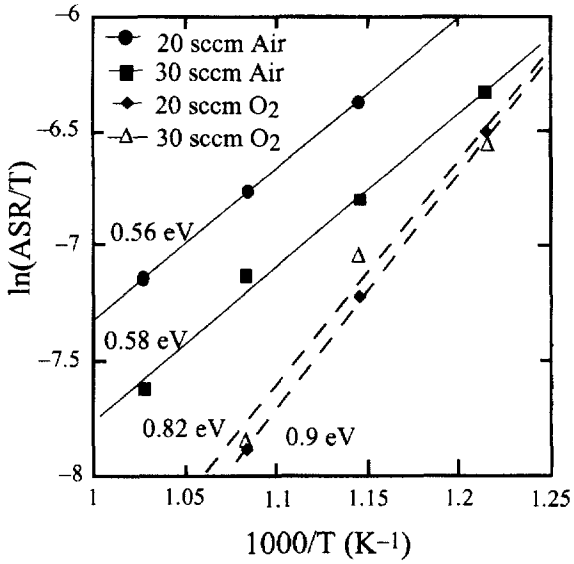


Fig. 15. ln(ASR/T) vs. 1/T of the cell.

polarization at the electrodes, which reduces on going to higher temperatures. Figure 12 shows the power density of the cell with air at the cathode which has been extrapolated to higher current densities. The power density of the cell was calculated with respect to the cathode area. At 650 °C with a flow rate of 30 sccm, the cell showed a measured power density of 0.24 W/cm$^2$ at a current density of 0.4 A/cm$^2$. At 650 °C, the extrapolated power density is about 0.27 W/cm$^2$ at 0.62 A/cm$^2$. This is comparable to power densities reported in the literature for thick film ceria IT-SOFC [19,20].

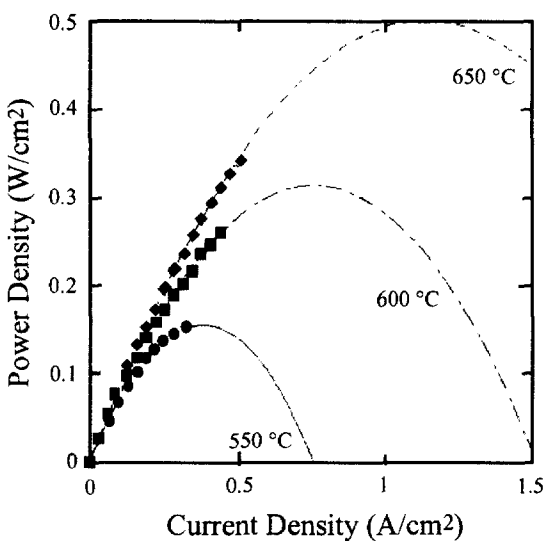


Fig. 14. Power Density of the cell with oxygen at the cathode.

The performance of the cell was compared with oxygen at the cathode. Similar trends were observed in the I-V characteristics and power density of the cell with oxygen at the cathode as shown in Fig. 13 and Fig. 14, respectively. The cell with oxygen showed a higher measured power density (0.29 W/cm$^2$ at 0.4 A/cm$^2$, 650 °C) compared to air at cathode. At 650 °C, the extrapolated power density is about 0.5 W/cm$^2$ at 1.14 A/cm$^2$. Due to the asymmetric size of the electrodes, the measured power densities values could have been over-estimated. However, as pointed out by Jiang et al. [21] in the case of anode supported cells these over-estimations are generally small.

Figure 15 is a plot of ln(ASR/T) vs. 1/T with air and oxygen at the cathode with different flow rates. Area specific resistance (ASR) of the cell is calculated from the slope in the ohmic region of the I-V plots. With air at cathode, on increasing the flow rate there is significant decrease in the ASR but with similar activation energies (~0.58 eV). For example at 650 °C, ASR of the cell decreased from 0.77 Ωcm$^2$ to 0.47 Ωcm$^2$ on increasing the air flow rate from 20 sccm to 30 sccm. With oxygen there is further decrease in the ASR but without much effect of flow rate and with a higher activation energy (~0.82 eV) compared to that of air. At 650 °C, ASR of the cell with oxygen was about 0.35 Ωcm$^2$ for both the flow rates. This suggests that there are two different rate limiting processes which are determining the cell performance when operating with air and oxygen at the

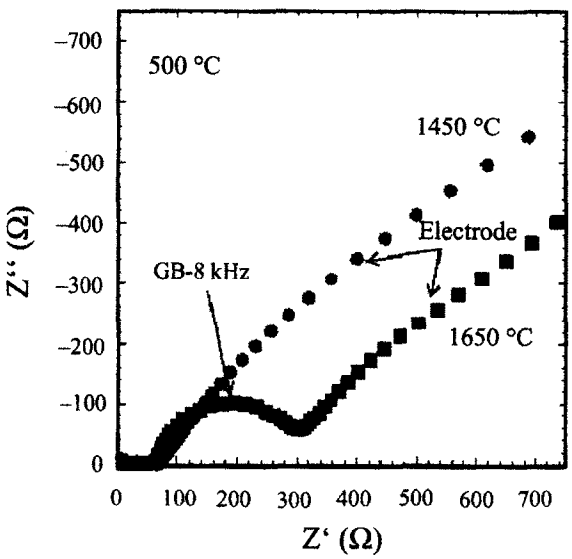


Fig. 16. Impedance plots at 500 °C for GDC electrolyte sintered at 1450 °C and 1650 °C.

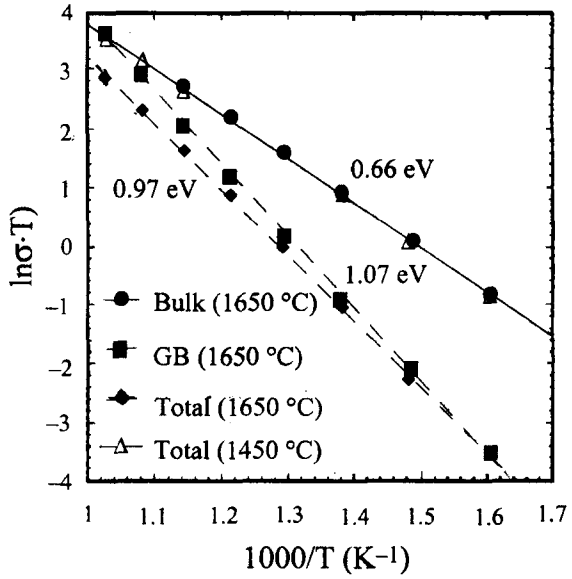


Fig. 18. Arrhenius plot of oxygen ion conductivity-bulk, grain boundary (GB) and total for GDC electrolyte sintered at 1450 °C and 1650 °C.

cathode. With air, the effect of flow rate and a lower activation energy suggests that the rate limiting step is the gas diffusion at the relatively dense, ~85 μm thick cathode. With oxygen, oxygen ion transport across the electrolyte seems to be the rate limiting step as found by impedance spectroscopy studies described below.

Impedance plots of symmetrical cells with GDC electrolyte and Pt electrodes at 500 °C and 700 °C are shown in Fig. 16 and 17, respectively. The GDC electrolyte was sintered at two different temperatures:

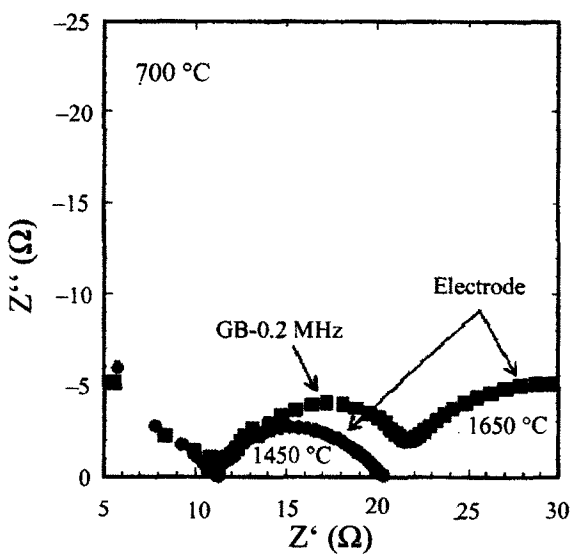


Fig. 17. Impedance plots at 700 °C for GDC electrolyte sintered at 1450 °C and 1650 °C.

1450 °C and 1650 °C. The contributions of the electrolyte (bulk and grain boundary) and electrode are separated in the impedance spectra due to different relaxation time constants. The electrolyte sintered at 1650 °C showed both bulk and grain boundary arcs and a higher total resistance compared to the electrolyte sintered at 1450 °C, which did not show the grain boundary arc. Arrhenius plots for the macroscopic bulk, grain boundary and total conductivity of the GDC electrolyte are shown in Fig. 18. Macroscopic conductivity is calculated from the sample thickness and cross-section area. Activation energy of the bulk conductivity for both the sintering conditions are ~0.66 eV; for 1450 °C, bulk conductivity is equal to the total conductivity. Grain boundary activation energy for the electrolyte sintered at 1650 °C is ~1.07 eV, which results in much higher activation energy of ~0.97 eV for the total conductivity. GDC powder from Rhodia has very low $SiO_2$ impurities (<30 ppm) and is expected to have low or negligible grain boundary resistance [22], which is the case for the electrolyte sintered at 1450 °C. For the electrolyte sintered at 1600-1650 °C, $SiO_2$ contamination from the $MoSi_2$ furnace elements during sintering (confirmed by EDS) has resulted in high grain boundary resistance. Microscopic or specific grain boundary conductivity, taking into consideration the grain boundary thickness, is in fact ~3 orders lower than the macroscopic grain boundary conductivity. Presence of $SiO_2$ impurities at grain boundary

is detrimental and resulted in lower magnitude and higher activation energy for the total conductivity, which appears to be the rate limiting step for the cell with oxygen at the cathode. Therefore, the final sintering temperature of the electrolyte/anode bilayer has to be lowered to avoid $SiO_2$ contamination, which not only reduces the electrolyte conductivity but is also known to affect the electrode performance [23].

In cells with ceria electrolyte, the power density depends on the conflicting parameters of cell potential and the ASR of the cell. On increasing the temperature, the cell potential decreases along with the ASR which would result in a critical temperature at which the maximum power density can be achieved from the cell. This critical temperature seems to be greater than 700 °C. By depositing an electron blocking and high oxygen ion conducting layer of stabilized bismuth oxide on the cathode side of the doped ceria electrolyte, we have shown that open circuit potential can be improved without increasing the ASR of the cell [24]. Thus, this limitation could be overcome resulting in improved SOFC performance at intermediate temperatures.

## 4. Conclusion

Ni-GDC anode supported thick film GDC electrolyte fuel cell was fabricated by a colloidal deposition technique. The density of the film depends on the sintering schedule – the pre-sintering and the final sintering conditions. Unit cells were fabricated with LSCF as cathode and tested in a fuel cell configuration. The performance of the cell in the open and closed circuit conditions was comparable to the performances reported in the literature. With air at the cathode, the performance of the cell seems to be limited by gaseous diffusion in the cathode and with oxygen by oxygen ion transport across the electrolyte. Further, it is expected that deposition of an electronically blocking layer of stabilized bismuth oxide layer on the doped ceria electrolyte will result in improved performance at intermediate temperatures.

## 5. References

[1] B.C.H. Steele, Solid State Ionics **134**, 3 (2000).

[2] B.C.H. Steele, Journal of Materials Science **36**, 1053 (2001).

[3] J.M. Ralph, A.C. Schoeler, M. Krumpelt, Journal of Materials Science **36**, 1161 (2001).

[4] R. Doshi, V.L. Richards, J.D. Carter, X.Wang, M. Krumpelt, J. Electrochem. Soc. **146**, 1273 (1999)

[5] H. Inaba, H. Tagawa, Solid State Ionics **83**, 1 (1996).

[6] J.B. Goodenough, Annual Review of Materials Research **33**, 91 (2003).

[7] K. Zheng, B.C.H. Steele, M. Sahibzada, I.S. Metcalfe, Solid State Ionics **86**, 1241 (1996).

[8] J. Will, A. Mitterdorfer, C. Kleinlogel, D. Perednis, L.J. Gauckler, Solid State Ionics **131**, 79 (2000).

[9] S. de Souza, S.J. Visco, L.C. De Jonghe, J. Electrochem. Soc. **144**, L35 (1997).

[10] J.W. Kim, A.V. Virkar, K.Z. Fung, K. Mehta, S.C. Singhal, J. Electrochem. Soc. **146**, 69 (1999).

[11] S. Ohara, R. Maric, X. Zhang, K. Mukai, T. Fukui, H. Yoshida, T. Inagaki, K. Miura, Journal of Power Sources **86**, 455 (2000).

[12] L.W. Tai, M.M. Nasrallah, H.U. Anderson, M.A. Alim, J. Electrochem. Soc. **142**, 491 (1995).

[13] B.C.H. Steele, J.M. Bae, Solid State Ionics **106**, 255 (1998).

[14] E. Perry Murray, M.J. Sever, S.A. Barnett, Solid State Ionics **148**, 27 (2002).

[15] B.C.H. Steele, Solid State Ionics **75**, 157 (1995).

[16] L.W. Tai, M.M. Nasrallah, H.U. Anderson, D.M. Sparlin, S.R. Sehlin, Solid State Ionics **76**, 273 (1995).

[17] K.T. Miller, F.F. Lange, D.B. Marshall, Journal of Materials Research **5**, 151 (1990).

[18] P.H. Middleton, M.E. Stirsen, B.C.H. Steele, in: Proceedings of 1st Int. Symp. Solid Oxide Fuel Cells (S.C. Singhal, Ed.) The Electrochemical Society Proceeding Series, Pennington, NJ, 1989, p. 90.

[19] M. Sahibzada, B.C.H. Steele, D. Barth, R.A. Rudkin, I.S. Metcalfe, Fuel **78**, 639 (1999).

[20] C. Xia, F. Chen, M. Liu, Electrochemical and Solid-State Letters **4**, A52 (2001).

[21] Y. Jiang, A.V. Virkar, F. Zhao, J. Electrochem. Soc. **148**, A1091 (2001).

[22] B.C.H. Steele, Solid State Ionics **129**, 95 (2000).

[23] J.M. Bae, B.C.H. Steele, Solid State Ionics **106**, 247 (1998).

[24] E.D. Wachsman, P. Jayaweera, N. Jiang, D.M. Lowe, B.G. Pound, J. Electrochem. Soc. **144**, 233 (1997).

*Manuscript rec. Feb. 14, 2005; acc. March 17, 2005.*